UPPSALA
UNIVERSITET

Effect of Electronic Exchange-Correlation Interaction in the Physics of Ion Insertion in Organic Salts

Mirna Alhanash

Supervisor: Moyses Araujo

Project in Physics and Materials Science
Uppsala University

UPPSALA
UNIVERSITET

Table of Contents

Abstract

The intense increase in energy consumption around the world has prompted a great deal of research on alternative and sustainable energy storage systems such as organic batteries. The fundamental understanding of the physics of organic salts and the ion insertion mechanism plays a key role in the development of electrode materials used in such sustainable batteries. The system studied in this project is of Lithium (2,5-dilithium-oxy)-terephthalate where a previous project studied this system from a different angle. The electronic structure generation of the system is based on Density Functional Theory (DFT) along with an evolutionary algorithm to find the structures with minimum energy. The effects of varying the description of the exchange-correlation interaction were studied while introducing lithium ions to the system. This was done while also monitoring the repercussions of crystal structure optimization on the voltages, charge redistribution, and bonds of the system. The geometrical optimization of the hybrid functional resulted in the potential of the 2-electron step between Li_2-p-DHT/ Li_4-p-DHT of 2.6 V being closer to the experimental value recorded at 2.7 V.

I. Introduction

Lithium-ion batteries (LIBs) have proven to be a revolutionary energy storage technology due to their high gravimetric energy density and substantial potential which was a great upgrade from older battery models. Since energy consumption is always on the rise, these LIBs have been increasingly in demand to keep on with such growth. While this surely has some advantages, it raises some concerns about the sustainability part of the inorganic sourced lithium-ion batteries. There is numerous research on the field of renewable energy with their eyes set to produce efficient alternative energy. Therefore, in order to match the sustainability goals for renewable energy sources, an environmentally friendly energy storage system should be efficiently developed as well.

This is why organic batteries have been greatly investigated as a promising alternative due to their interesting properties. Organic electrode materials present great advantages coming from renewable sources from the biomass thus being cost-efficient while showing promising gravimetric capacity. The use of transition metal electrode materials in today's batteries comes at a greater cost than just the economical one. These materials are heavily mined which could lead to source depletion dragging along other geopolitical dilemmas. The production process is also environmentally harmful because of the strenuous synthesis of materials and low recyclability [1,2]. Organic electrode materials show promising ground for future research because of their tunable properties with materials design yet exploring the different molecules to be used in all organic batteries have proven challenging. This is due to the difficulties it poses to synthesize them experimentally and thus studying them which presents a lack of data on the varied pool of choices. Therefore, computational methods play a vital role in such material discovery by screening for possible materials to be used in future green batteries. This is done by predicting the thermodynamics and crystal structures of materials to understand how to effectively use them in modern-day sustainable batteries.

A previous research project was done on the atomic scale modeling of Lithium (2,5-dilithium-oxy)-terephthalate to be used as organic electrode materials, showing the structure in Figure [1]. Electronic structure calculations were performed on the pristine structure and after inserting lithium ions step-wise up to four ions. After predicting the crystal structure and calculating the voltage for the system using a DFT calculation, a full

analysis was done by constructing the density of states and Bader charge analysis to study the electron delocalization in the system. These thermodynamic properties and charge distribution are important in order to understand the material's electric properties and see structure evolution through ion insertion.

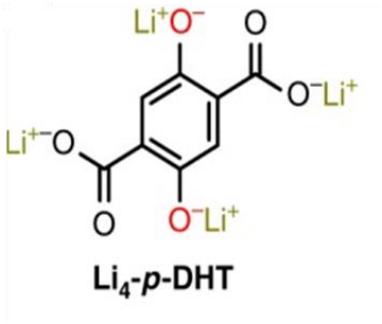

Figure [1]: Lithium (2,5-dilitium-oxy)-terephthalate structure [3]

Some of the observations found in the results of the previous project are that the voltage profile generated by the geometrically optimized generalized gradient approximation (GGA) was different from the ones calculated through the non-geometrically optimized Heyd, Scuseria, and Ernzerhof (HSE) hybrid functional. The latter showed a higher deviation from the experimental result of 2.6 V with a value of 3.11 V for the two-electron step between Li_2-p-DHT/ Li_4-p-DHT. The experimental potential was recorded by Wang et al. of the aforementioned structures in the form of nanosheets [4]. This raised some questions regarding the effects of exchange-correlation interaction fraction on the crystal structure and lithiation mechanism. In order to explore the fundamental understanding of the physics of ion insertion in such organic salts, a study on the exchange-correlation interaction and geometrical optimization over different functionals and their effects was carried out. The use of different functionals to solve for the electronic exchange-correlation provides different approximations that could sometimes be an overestimate or underestimate depending on the fraction of the exact exchange from Hartree Fock (HF) used. A local density approximation (LDA) for example shows an overestimation of the exchange energy due to the electrons' self-interaction. Thus, the first aim of this research is to focus on varying the exchange-correlation energy fraction for the different lithiation steps. The other is to compare the effects of geometrical optimization of HSE hybrid functional on the crystal structure and thermodynamics of Li_x-p-DHT since it is a two-

electron reaction, where a single step radical formation could affect the geometry of the structure [3,4].

II. Theory

Density Functional Theory (DFT)

In the materials realm, the information about their electronic structure and thermodynamics offers a key to conquer their secrets by allowing us to better understand their properties and design different functional materials. While solving for a one-electron system is relatively easy, using a detailed quantum mechanical calculation to simulate materials with many electrons and find their electronic structure would take enormous memory and a very long time to compute because of the many-body problem. Therefore, a more mathematical approximation would be needed for a material's computation that is both reasonably accurate and time-efficient. That is why the triumphant Density Functional Theory (DFT) was a breakthrough in the materials world especially after the 90s where better hybrid functionals and exchange correlations were under development. This computationally supported quantum mechanical model has provided a tool for many world-leading researchers to predict and design novel materials under different conditions as well as better understand other ambiguous materials by predicting their ground state energy and thus finding their thermodynamical properties. DFT, therefore, has proven useful in many different fields of chemistry, physics, condensed matter, and materials science. The concept that DFT is based on, is that instead of working with individual electrons in a quantum mechanical system using wavefunctions, a cloud of electrons is considered [5]. The advantage of envisioning an electron gas density is that the density of electrons remains a three-dimensional quantity represented as a field regardless of how many electrons are involved [6].

In order to better understand density functional theory, it would be necessary to understand its quantum mechanical background. The complete information about a system is encapsulated in its wave function Ψ represented in the known Schrödinger equation with the E as the eigenvalue of the system's energy,

$$\hat{H}\Psi = E\Psi \quad (1)$$

Since the system is large and contains electronic and nucleic parts, the first simplification to the system is to apply the Born-Oppenheimer approximation [7]. This approximation decouples the wavefunction into separate electron positions and nuclear positions due to the nuclear motion being very slow in comparison to the fast electrons and thus seen as a blurry potential. This is then represented in the Schrödinger equation for many-electron systems as follows,

$$\left[\sum_{i}^{n}\left(-\frac{\hbar^2\nabla_i^2}{2m}+v(r_i)\right)+\sum_{i<j}U(r_i,r_j)\right]\Psi(r_1,r_2,\ldots,r_N)=E\Psi(r_1,r_2,\ldots,r_N) \tag{2}$$

The main focus of this model is to solve for the hamiltonian where one could see three distinct terms represented by the kinetic energy $\hat{T}$, the internal potential energy $\hat{U}$, and the external potential energy $\hat{V}$ [6]. These different contributions of the hamiltonian are shown in the following equations [8],

$$\hat{T}=-\frac{\hbar^2\nabla_i^2}{2m}\sum_{i}\nabla_i^2 \tag{3}$$

$$\hat{U}=\sum_{i<j}U(r_i,r_j)=\sum_{i<j}\frac{q^2}{|r_i-r_j|} \tag{4}$$

$$\hat{V}=\sum_{i}v(r_i)=\sum_{i}\frac{Q_q}{|r_i-R|} \tag{5}$$

Thus, through calculating the expectation value of the Hamiltonian the electronic energy E_e will be obtained,

$$E_e=\langle\Psi_e|\hat{T}+\hat{U}+\hat{V}|\Psi_e\rangle=T+U+V=F+V \tag{6}$$

F is represented here as the sum of T and U and is considered the total internal electronic energy. The last terms are considered as the scalar expectation values of their designated operators. The challenges yet persist at this stage due to the large space where the dimensionality corresponds to the number of electrons involved in the system, this is where DFT solves such a problem by reducing the investigation into three-dimensional functions [6].

As it was mentioned before, density functional theory brings a different way to look at the wavefunctions where it introduces the electron density $n(r)$ of which its integral produces the total number of electrons. DFT acknowledges that the nonrelativistic Coulomb system is dependent only on their potential $v(r_i)$ and thus uses electron density to help solve the universal operators $\hat{T}$ and $\hat{U}$, where the latter is mapped onto a single body problem without the operator [8]. While external energy $\hat{V}$ is rewritten in terms of the density as a functional. A functional is described as a linear mapping from an object into a function producing a scalar. The potential energy functional is denoted as V[n] of the electron density and this along with the other functionals are thus called density functionals [6]. This yields in the rewrite of the electronic energy as functionals of the wave function Ψ_e,

$$E_e = T[\Psi_e] + U[\Psi_e] + V[v,n] = F[\Psi_e] + V[v,n] \tag{7}$$

Then the theory developed to rewrite the total internal energy $F[\Psi_e]$ as a functional of the density F[n] using the Thomas-Fermi model seen in equation [6],

$$E_e \approx T_{TF}[n] + J[n] + \int n(\boldsymbol{r})\, v(\boldsymbol{r})\, d\boldsymbol{r} \tag{8}$$

$$F[n] \approx T_{TF}[n] + J[n] \tag{9}$$

Where equation (8) shows the total kinetic energy $T_{TF}[n] \approx T$ and the internal potential energy U is approximated using the electrostatic energy of a classical repulsive gas J[n] [6].

Kohn-Sham Equations

In order to solve the previous equation, one first considers a system without electron-electron interaction thus focused on solving functionals T for the kinetic energy and V_s for the effective potential. This is where the famous Kohn-Sham equations offer an approach to solve for the ground state energy of a many-body system using a single particle orbital representation Ψ_i yielding Kohn-Sham orbital energies ϵ_i [9],

$$-\left(\frac{\hbar^2}{2m}\right)\nabla_i^2\Psi_i(r) + v_{eff}(r)\Psi_i(r) = \epsilon_i\Psi_i(r) \tag{10}$$

This then produces the expression of the particle density,

$$n(r) = \sum_{i=1}^{N} |\Psi_i(r)|^2 \tag{11}$$

The single-particle energy is shown as,

$$E_s = \sum_i \epsilon_i \tag{12}$$

In order to correct for the electron-electron interaction, the effective single-particle potential uses an exchange-correlation potential v_{xc} that counts for them. Since the terms in the following equation are dependent on each other, Kohn-Sham equations are calculated self-consistent field (SCF).

$$V_s(r) = v(r) + \int \frac{n(r')}{|r - r'|} dr' + v_{xc} \tag{13}$$

This exchange-correlation potential is where the different approximation methods used in computational processes are distinguished and is the partial focus of this research. Finally, DFT in general uses an electron density minimization process that produces the ground state energy, a summary is shown in Figure [2].

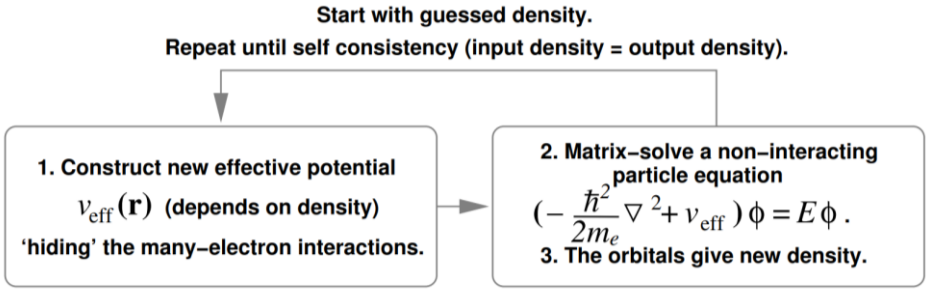

Figure [2]: A summary of the Kohn-Sham electron density minimization using a self-consistent solution [6].

Exchange correlation XC and example functionals

Ground state energy calculations in DFT are mostly done through the Kohn-Sham equations where this is commonly a fixed part of the computational process, the option variation comes from a specific term approximation. A vital criterion on which a computational method is chosen is the exchange-correlation (XC) potential approximation. There are different types of approximations with different levels of theory or accuracy that are used depending on the specific system to be computed. These

different density functional approximations for XC are usually classified in a "Jacob's ladder" where the top of the ladder reaches functionals with the highest-level accuracy. The earliest approximation for the XC potential that lies at the bottom of the ladder is the local density approximation (LDA). In this approximation at position r, the exchange-correlation energy density is dependent only on the particle density $n(r)$[10]. An important factor that density functionals need to satisfy is the exchange-correlation hole. This describes an area around a particle where it will be less likely to find an identical particle there due to the Pauli exclusion principle, which LDA satisfies. A very common functional used is the generalized-gradient approximation (GGA) such as Perdew, Becke, and Ernzerhof (PBE) functionals, which is used in the research project but supported with other functionals like HSE hybrid functional due to the former's overestimation of the electron delocalization which arises from the unphysical electron self-interaction [10, 11].

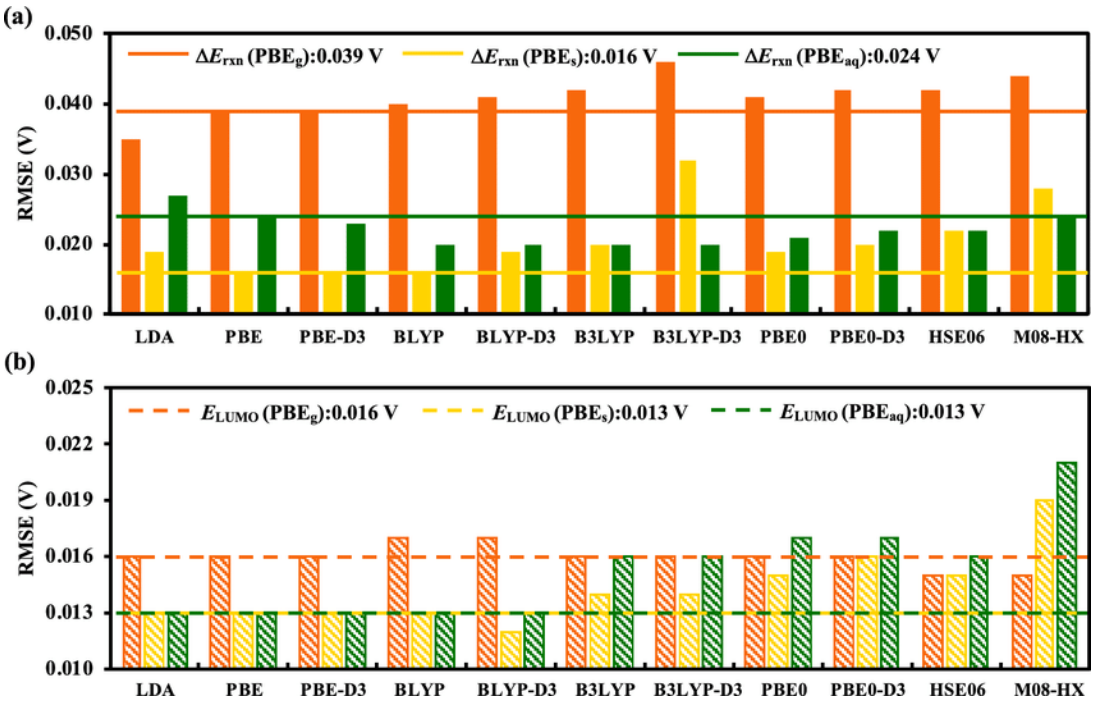

Figure [3]: A comparison in the performance of the different exchange-correlation XC approximation functionals. [12]

With higher levels of theory, as well as computational time, some functinals go at the top of the ladder like meta GGAs and hybrid functionals. Figure [3] shows a comparison in the performance between the different functionals, this research used HSE hybrid functional which will be further discussed.

Heyd–Scuseria–Ernzerhof (HSE) Hybrid Functional

One type of previously mentioned functionals that is an improvement from GGA is considered to be hybrid functionals. The reason such functionals offer a better prediction for band gaps -specifically metals- is that they include the "non-dynamical correlations that delocalize the GGA exchange hole" successfully. These hybrids are calculated using Gaussian-type orbitals and periodic boundary conditions (PBC) [13,14]. The strategy used in PBC for the long-range coulombic interactions problem is based on the direct space fast multipole method (FMM), however, this could not be used for HF. In insulators, Walter Kohn showed that the range of the exchange interaction decays exponentially as a function of the HOMO–LUMO energy difference, however, for systems with small band gaps this decay appears to be algebraic [9,14]. Since hybrid functionals include a portion of Hartree Fock (HF) exchange, it is important to obtain a technique of which is able to calculate the Hf exchange without having a long and expensive computational process, especially for larger systems. HF is normally computationally challenging to produce since it is calculated as a "sum over all significant interactions in the unit cell and between the unit cell and its neighbors" in real space, this results in a slow convergence with distance in metallic systems along with problems in the self-consistent field (SCF) [15]. In regards to metallic systems, a divergence in HF calculations appears in the derivative of the orbital energies with reference to *k*. This is due to the 1/r Coulomb potential's Fourier transform where it diverges at $k = 0$. A new approach by Heyd, Scuseria, and Ernzerhof (HSE) utilizes the long researched screening of the Coulombic potential of a shorter range than 1/r potential in order to get rid of the divergence [14]. The authors' new technique is to use this screened Coulomb potential only to the exchange interaction, specifically to be used in HF exchange as a way to screen for the long-range part. This means that using an error function for the Coulomb operator, splits it into different parts of short-range (SR) and long-range (LR) as seen in the next equation, and therefore a screened potential will not be used to the other Coulomb interactions of the Hamiltonian [14].

$$\frac{1}{r} = \frac{erfc(\omega r)}{r} + \frac{erf(\omega r)}{r} \tag{14}$$

The first part of the equation is short-range and the second is the long-range with erfc(ωr)=1- erf(ωr) with a varying ω. This screened Coulomb potential aids in shifting the exchange energy decay as a function of distance to an exponential decay for small to no bandgap systems as shown in Figure 4 [14].

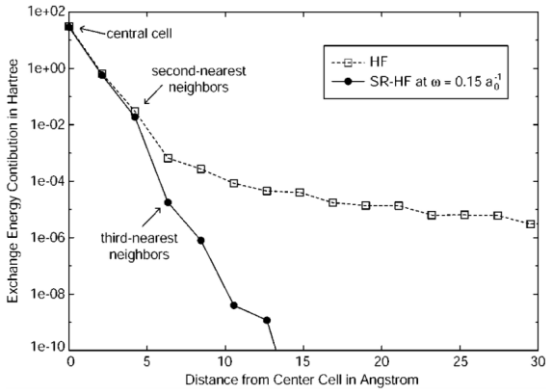

Figure [4]: The HF exchange energy part decay as a function of distance from the reference cell in a metallic system. The squares represent a non-screened system and circles, a short-range HF exchange [14].

The HSE hybrid functional finds the exact exchange for the short-range interactions while neglecting the long-ranged ones in HF and DFT. The long-range interactions are however corrected by replacing it with Perdew–Burke-Ernzerhof (PBE) long-range where HSE is based on the PBE0 hybrid exchange-correlation functional created by Ernzerhof et al [16,17] that is part PBE and part HF. This occurs when the exchange-correlation energy terms are split into short and long-range, where the long-range exchange involvement in HF and PBE is very small that these terms cancel each other. If these terms are neglected and compensated by other terms in the functional, the following exchange-correlation energy produced by a screened Coulomb potential hybrid density functional is shown [14,15],

$$E_{xc}^{\omega PBEh} = \alpha E_x^{HF,SR}(\omega) + (1-\alpha)E_x^{PBE,SR}(\omega) + E_x^{PBE,LR}(\omega) + E_c^{PBE}(\omega) \qquad (15)$$

Where realistic ω values were chosen as a variable controlling short-range interactions of such ω= 0.15 α_0^{-1} that provided a good combination of accuracy and speed. The long and short-range interactions for PBE and short-range interactions for HF are denoted in the equations and α = ¼ representing the HF mixing coefficient. At ω = 0 the ωPBEh, or later referred to as HSE, corresponds to PBE0, and at ω → infinity, it reaches PBE [14].

An important part that differentiates the types of hybrid functionals is the approach used for the exchange-correlation correction and thus to understand the HSE hybrid functional, one needs to understand where the exchange energy comes from. The long-range ωPBE hybrid is compensated by combining terms from PBE and ωPBE, SR exchange energy density. While the short-range terms, as mentioned before, include a screened Coulomb potential for both HF and PBE. For the latter, the exchange hole from PBE is used as a starting point and then scaled by a short-range Coulomb screening factor. It is then enhanced not only by the SR Coulomb screening but also with a correction to local density approximation (LDA) using PBE gradient [14]. This results in the short-range ωPBEh exchange energy density as follows,

$$\epsilon_x^{\omega\mathrm{PBE,SR}}(\rho(r), s(r)) \;=\; \epsilon_x^{\mathrm{LDA}}(\rho(r)) F_x^{\omega\mathrm{PBE,SR}}(\rho(r), s(r)) \tag{16}$$

The authors Ernzerhof et al. then used the former result and integrated it over all space, yielding the following exchange energy part from the short-range ωPBE,

$$E_x^{\omega\mathrm{PBE,SR}}(\rho(r), s(r)) = \int dr\, \rho(r) \epsilon_x^{\omega\mathrm{PBE,SR}}(\rho(r), s(r)) \tag{17}$$

Lastly, the beforementioned long-range ωPBEh is shown in the following equation with the compensated terms from the functional,

$$E_x^{\omega\mathrm{PBE,LR}}(\rho(r), s(r)) \tag{18}$$
$$= \int dr\, \rho(r) [\epsilon_x^{\mathrm{PBE}}(\rho(r), s(r)) - \epsilon_x^{\omega\mathrm{PBE,SR}}(\rho(r), s(r))$$

The HSE hybrid functional therefore offers a great improvement from PBE due to the modifications that result in a faster convergence for the short-range HF part and a refined response in self-consistent-field (SCF).

	G2-1 set[b]			
Method	MAE[d]	RMS[e]	Max.(−)[f]	Max.(+)[g]
B3LYP	2.46	3.28	−8.2	9.9
PBE	8.19	10.40	−29.1	10.1
PBE0	3.01	3.76	−6.1	10.6
ωPBEh	2.93	3.78	−7.2	10.7
	G2-1andG2-2set[c]			
Method	MAE	RMS	Max.(−)	Max.(+)
B3LYP	3.04	4.40	−8.2	20.0
PBE	17.19	21.00	−50.8	10.1
PBE0	5.15	6.78	−20.8	21.7
ωPBEh	4.16	5.68	−17.4	20.5

[a]6-311++G(3*df*,3*pd*) basis set.
[b]55 molecules.
[c]148 molecules.
[d]Mean absolute error.
[e]Root mean square error.
[f]Maximum negative deviation.
[g]Maximum positive deviation.

Table I: A comparison between different hybrid functionals results for the mean absolute error of the enthalpies of formation of two sets of systems [14]

A comparison between the enthalpies of formation for a set of 55 molecules and a larger system of 148 molecules with enthalpies of formation at 298 K [18] using different functionals of higher and lower accuracies and computational time are shown in Table I. The table shows a mean of absolute errors generated for the enthalpies in the same main ωPBEh paper, explaining that this functional offers a great prediction for systems' thermodynamics and matches some of the best hybrid functionals in accuracy [14].

III. Computational Methods

The main process of this computational research was to first generate a crystal structure using the USPEX and Vienna ab-initio simulation package (VASP) codes. This was done using an evolutionary algorithm (EA) in USPEX to generate different structures while utilizing VASP to perform DFT calculations to find the minimum energy for structures. The task of the evolutionary algorithm was to generate different generations of predicted structures based on designated qualities awarded by evaluation functions. Each generation contains a population of possible solutions where the initial one is a random combination of structures. This is then evolved by creating new generations using operations like a fitness function, heredity function, mutation function, and a selection function [19,20]. The main goal is to reach a structure candidate from an evolved generation

with a global energy minimum. A set of 40 generations were produced in USPEX for the different lithiated structures with an initial population size of 200-300. This initial population from Generation 0 is then filtered into smaller population sizes of 20 for the rest of the generations by choosing structures with lower energies from their DFT calculations along with other computed structures. The accuracy of the basis set is controlled by the E_{cut} which is set to be 600 eV for all functionals.

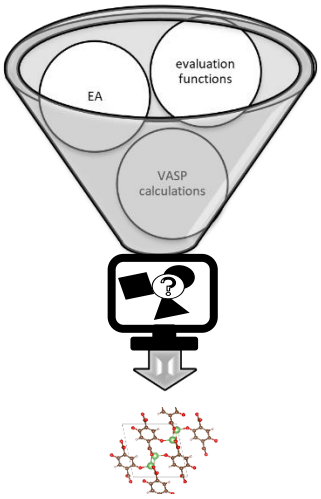

Figure [5]: An illustration showing USPEX involving evolutionary algorithm along with DFT calculations in VASP to compute crystal structures.

The data generated for structures using GGA functional from the previous research project was extracted and used in the new calculations for the different exchange-correlation percentages. A geometric optimization with a single gamma k-point (1x1x1) calculation was run for that data in both GGA and then HSE hybrid functional. For the final structure, an increase to (4x4x4) k-point with the data from the geometrically optimized structures was used to reduce the computational time by turning off the geometric optimization parameters for the higher k-points. This was done for all the pristine material and the different lithiated structures with varying the fraction of the exact exchange of HF-DFT and hybrid functional AEXX between 25-55% in steps of 10%. The density of states and Bader analysis were then generated for the 25% XC to compare it to the previous work of the non-optimized 25%.

IV. Previous Work

Previous research results on Li_x-p-DHT are incorporated in this study and compared to the newly generated data because it helps in understanding the physical mechanism,

charge distribution, the effects of geometrical optimization, and varying exchange-correlation on the system.

V. Result and Discussion

i. Crystal Structure

The crystal structure was generated for the delithiated structure Li_2-p-DHT as well as the different lithiation steps. Information about the molecular structure of the electrode material is important to understand where the ion insertion happens and to understand the geometrical changes in the system. The unit cell involved two molecules, therefore, each lithiation step involved two lithium ions with one ion reacting per benzene ring. Four lithiation steps were conducted with the insertion of a total of four ions between Li_2-p-DHT to Li_6-p-DHT. This was visualized using Vesta software from the data produced through two steps of a combined calculation of GGA and then HSE06 hybrid functional for each one. The aim of the first step was to optimize the geometry of the structures with fine single gamma points ending with an optimized hybrid functional. The second was to return to a higher K-points of (4x4x4) in order to compare the results within the same parameters with the previous research. This was done for different fractions of exchange-correlation (25%, 35%, 45%, 55%) for each structure, in this paper the crystal structures using only 25% will be shown. Figure [6] shows the previously mentioned structures where the evolution of the ion insertion and the accumulation of the salt layer in the middle is observed.

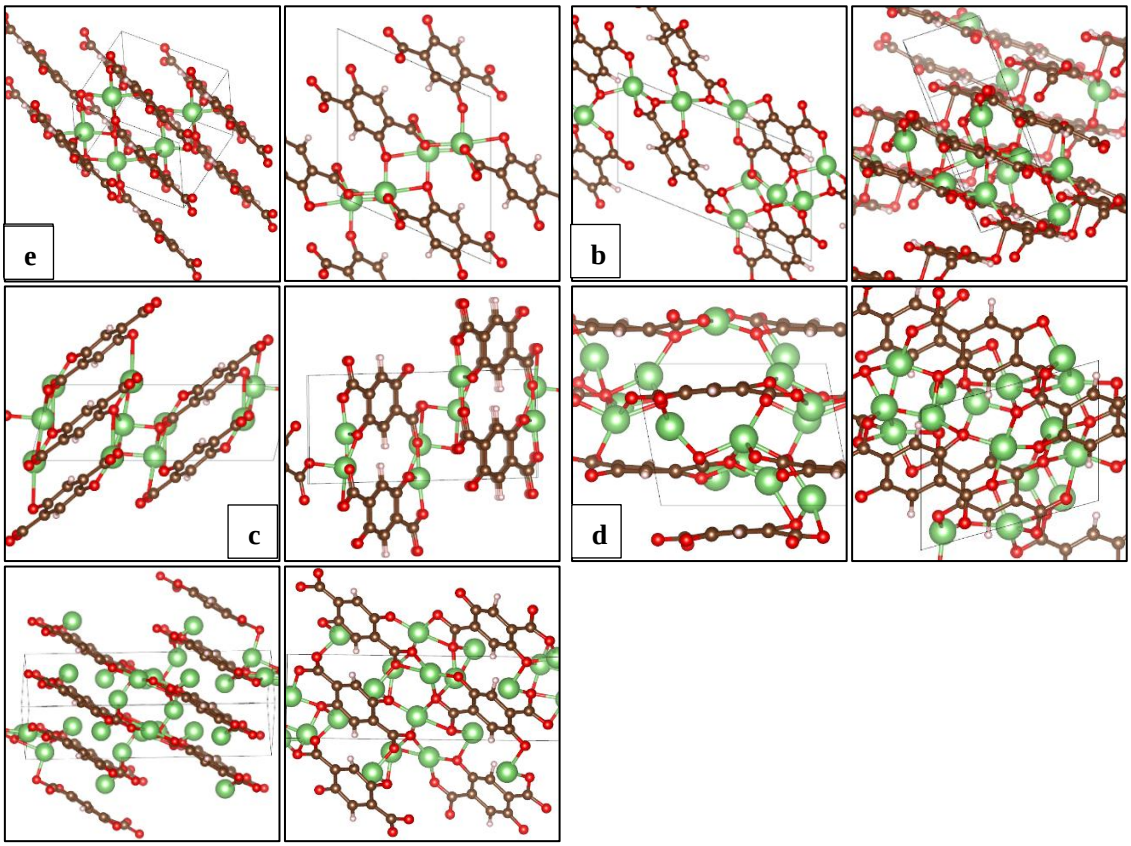

Figure [6]: The predicted crystal structure of the different lithiation steps for the geometrically optimized HSE06 with a 25% exchange-correlation fraction**. a)** Li_2-p-DHT **b)** Li_3-p-DHT **c)** Li_4-p-DHT **d)** Li_5-p-DHT **e)** Li_6-p-DHT

Geometry Optimization in HSE06 vs Non-geometry Optimization at 25% EC

A prominent observation was seen when the structures were compared between the ones that had the geometry optimization done for the hybrid functional step -steps mentioned previously- and between the ones that had geometry optimization in a (4x4x4) K-point GGA calculation but turned off for the hybrid functional step taken from previous work. When the structures were optimized with the HSE06 hybrid functional that has a better correction for the electrons self-interaction, they showed a slightly different distribution of the salt layer and another bond between one of the lithiums and the oxygen around the benzene ring. Figure [7] shows a comparison for the first two lithiation steps of the geometrically optimized HSE06 and the non-optimized structures from the previous work both in 25% XC fraction.

	Li_2	**Li_3**	**Li_4**
Non-Optimized (25%)	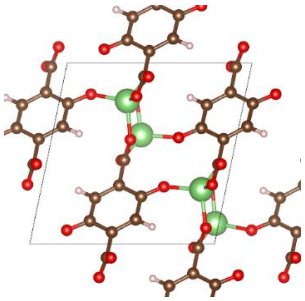	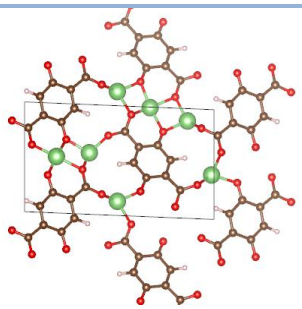	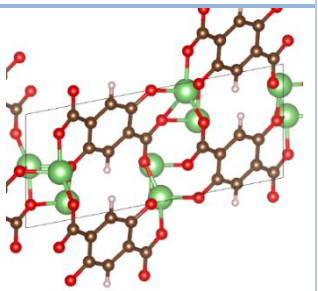
HSE06 Optimized	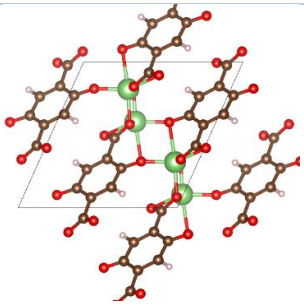	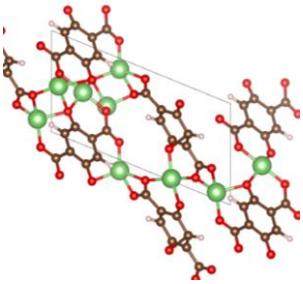	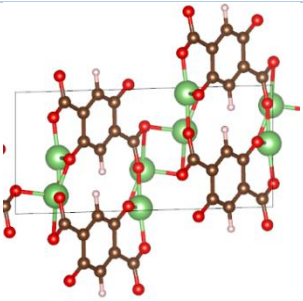

Figure [7]: A comparison between the crystal structures in the first two lithiation steps between Li_2-p-DHT/ Li_4-p-DHT from a geometrically optimized hybrid functional calculation and a non-optimized one both in 25% AEXX.

ii. Potential Energy / Voltage Profile

The lowest energies generated for the different lithiation steps aided in the calculation of the redox potentials of the different exchange-correlation fractions used. Two types of information are revealed looking at the voltages which are the effect of both the fraction of the exact exchange and the geometrical optimization in the hybrid functional step on the thermodynamical properties and crystal structure of the system.

Exchange correlation	*Li_2 Energy (eV)*	*Li_3*	*Li_4*	*Li_5*	*Li_6*
Non-HSE06 optimized 25%	-308.1620	-319.7391	-328.4876	-333.8734	-339.8910
25%	-306.9754	-314.8207	-325.6986	-333.7241	-338.2079
35%	-327.2010	-334.9409	-345.3596	-354.36011	-358.7165
45%	-347.6485	-355.3055	-366.0540	-375.2508	-379.4456
55%	-368.2773	-375.9944	-386.9383	-396.3866	-400.3699

Table II: The exchange-correlation fraction used for the lithiated and non-lithiated structures and their corresponding energies in eV.

POTENTIAL V/EXCHANGE CORRELATION	1ST LITHIATION LI 2 → 3	2ND LITHIATION LI 3 → 4	3RD LITHIATION LI 4 → 5	4TH LITHIATION LI 5 → 6
Non-HSE06 opt 25%	3.818	2.403	0.722	1.0379
2-step	3.1105		0.880	
25%	1.9518	3.4681	2.0419	0.271
2-step	2.7099		1.15644	
35%	1.8991	3.2384	2.5294	0.2073
2-step	2.5687		1.3683	
45%	1.8576	3.4033	2.6275	0.1265
2-step	2.6305		1.377	
55%	1.8877	3.5010	2.7533	0.0208
	2.6944		1.3870	

Table III: The exchange-correlation fraction used for the lithiated and non-lithiated structures and their corresponding voltages in V.

While most of the exchange-correlation fractions produce a voltage close to the experimental one of 2.6 V, the 45% fraction shows to be the closest result to the experimental output. The effects of the geometric optimization are once again seen here where the voltages seem to shift closer to the experimental value for the 25% fraction that has the geometry optimized in the hybrid functional showing a value of 2.7 V for the two-electron step. The potentials recorded from the previous research using a non-optimized HSE06 with a 25% fraction show an overestimate with a value of 3.1 V for the two-electron step. This could be due to the radical formation in a single-step reaction where a geometry optimization appears to be needed.

Another approach to visualizing the voltage profile of the different parameters studied is shown in Figure [8] where 8(a) shows the effects of the exchange-correlation fraction (25%-55%) on the voltage vs. Li+/Li for the two-electron reaction between Li_2-p-DHT/ Li_4-p-DHT and Li_4-p-DHT/ Li_6-p-DHT. On the other hand, Figure 8b shows the effect of the geometry optimization in HSE06 on the voltage where it generates more accurate results compared to the experimental value for the higher potential lithiation steps, however, it shows to be an overestimate for the lower potentials.

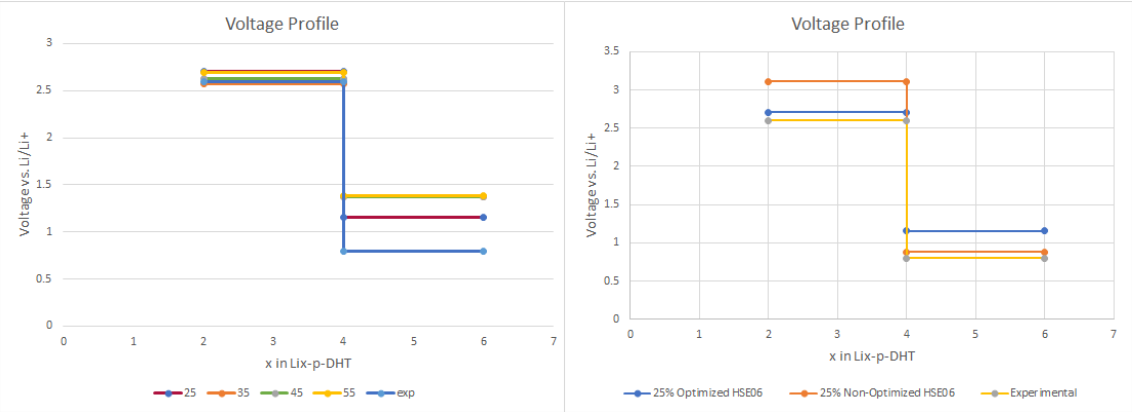

Figure [8]: **a)** Voltage profile of the 2-electron lithiation steps comparison of the different XC fraction and the experimental result. **b)** Voltage profile of the 2-electron lithiation steps focused on the geometrically optimized HSE06 and non HSE06 optimized vs experimental.

iii. Electronic structure

Due to the relatively large variety of exchange-correlation-related electronic structure data, a density of states (DOS) was generated only for the 25% fraction where the first two lithiation steps are shown in Figure [9]. The two sets of DOS both show similar behavior of the ion insertion effects. During the first two lithiation steps, a greater contribution from the oxygens connected to the rings and the benzene ring is observed where the former shows an inductive donor effect. The information from the density of states reveals information about the redox centers in the organic molecule, as was mentioned, in the first two lithiation where the higher potential redox centers of O and the ring act as cathode materials, the other one is seen to be the carboxylate group COO that acts as an anode due to its lower potential. This is seen in DOS where the contribution from the electron-donating COO- group becomes the most prominent after the saturation of the first redox centers, thus ions moving towards the carboxylates.

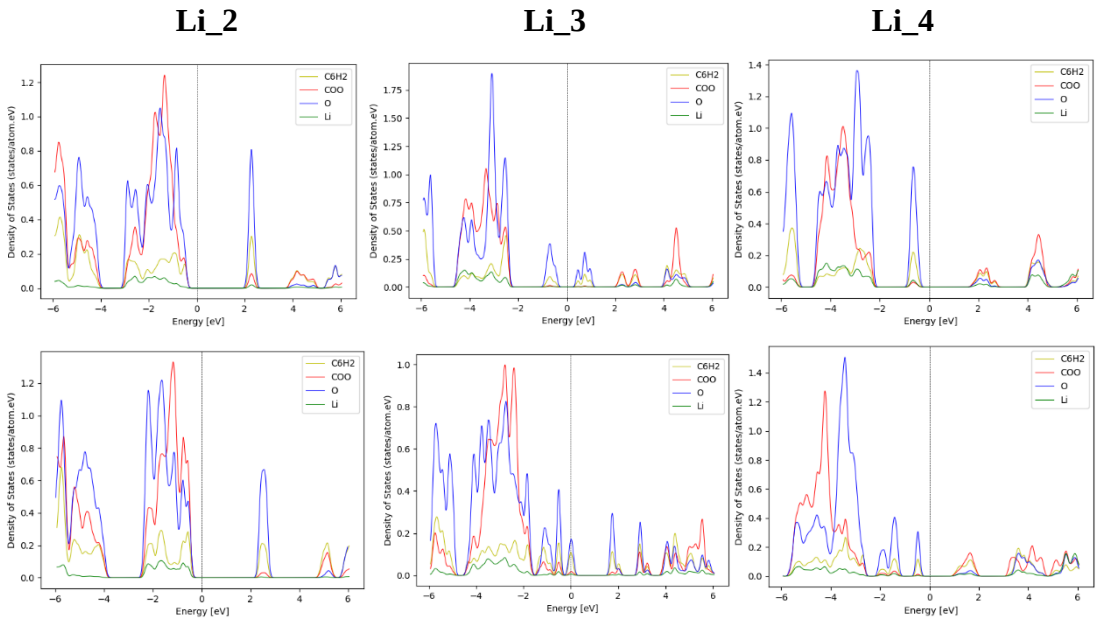

Figure [9]: The first line showing the density of states DOS for the first two lithiation steps for the non-HSE06 optimized structures. The bottom line showing the DOS of the geometrically optimized HSE06.

The electronic structure shows that the lithiation for this organic molecule appears as a two-electron step where there is a phase separation between Li_2-p-DHT and Li_4-p-DHT without having a clear intermediate step.

iv. Bader Analysis

A Bader charge analysis confirms the charge distribution results from the DOS where the total charge for the oxygen connected to the ring along with the ring has a high charge contribution at the first two lithiation steps and then decreases during the last two steps. This also shows the increase of the total charge for the carboxylate group for the final two lithiation steps.

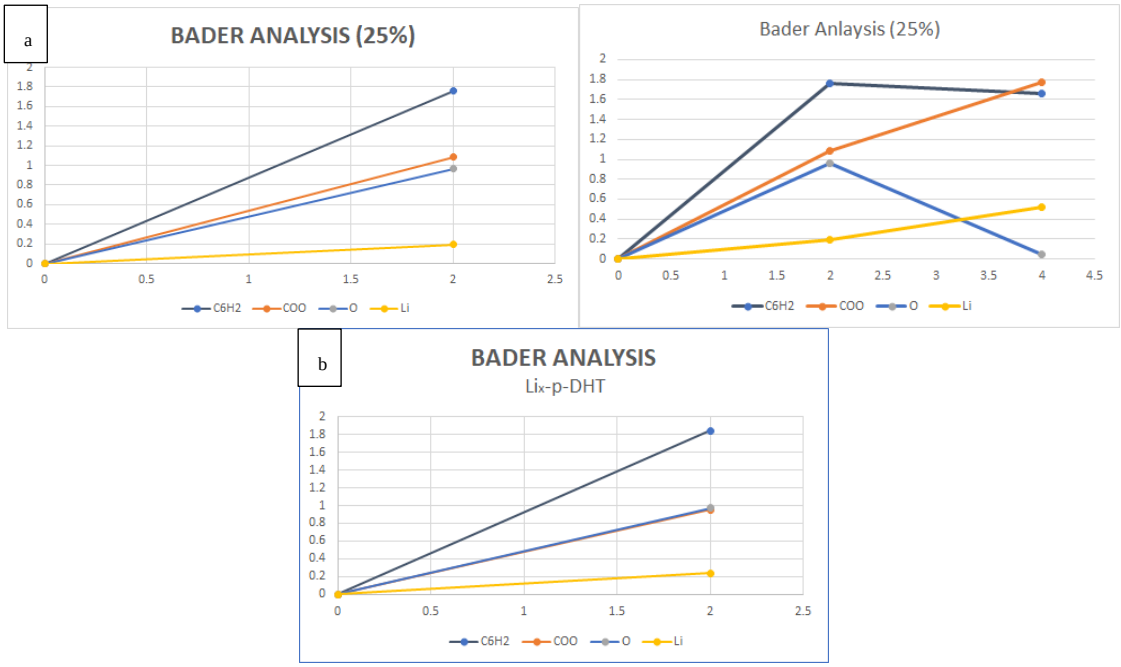

Figure [10]: A Bader charge analysis of the two 2-electron steps for the functional groups in the system based on a total electronic charge of atoms. Line a is the geometrically optimized system while b is the first two-electron step in the non-HSE06 optimized system.

v. Charge Density

A charge density visualization was generated using the partial charge density calculation. Figure [11] shows the charge density around the carbon ring of Li_4 of the geometrically optimized HSE06 hybrid functional and the non-optimized at the left. Both show a charge localization around the ring where it supports the notion that the two electron-donating groups COO^- and O^- are enriching the ring. This aids in understanding the tuning abilities of this system since controlling the stability of the p-electron density plays a key role in the increase of the potential energy of the system.

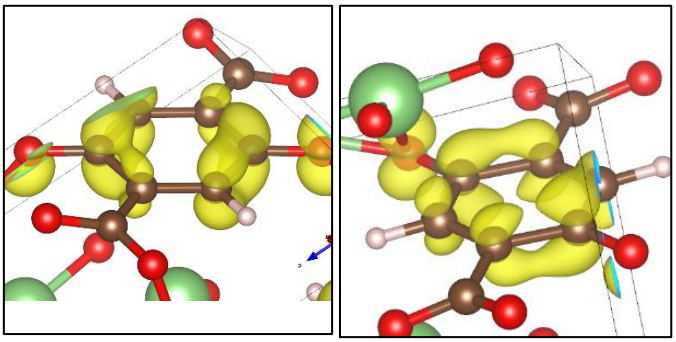

Figure [11]: left non-opt HSE06, right geometrically optimized HSE06

VI. Conclusion

Theoretical computation of possible electrode materials could assist in the optimization of synthetic methods and trials used in experimental research by filtering out materials with desirable properties that could yield high potential values in a battery cell, thus, saving efforts spent for following strenuous synthesis routes of different new compounds. Predicting the electronic structures of material reveals key information about their properties, specifically thermodynamically. Results from the previous research project raised some questions about differences in thermodynamical predictions in lithium terephthalate structures depending on the functionals used in DFT calculations which in turn led to questions about the fundamental physics mechanisms of organic salt ion insertion affected by computational method variation. These questions were explored in this project by studying the effects of i) exchange-correlation interaction variation on the thermodynamic properties of the system ii) Geometrical optimization of HSE06 vs non-optimization on the structure and thermodynamics of the system. Results correlated the difference of the exchange-correlation fraction used with slightly varied voltage output prediction of the structures. It seemed that using EC of 35% generated the closest voltage value of ~2.57V in the first two lithiation steps in comparison to the experimental voltage of 2.6V, although most fractions displayed very close results as well. Another important aspect investigated displayed information about the importance of geometrically optimizing the structures when using an HSE06 hybrid functional. This was due to the shift in voltage closer to the experimental value mentioned previously from 3.11V for a non-optimized calculation to 2.7V after optimizing in a 25% EC for both calculations. These observations from the analysis revealed the significance of geometrical optimization for the hybrid functional HSE06 for organic molecules, as well as the proper selection for an exchange-correlation fraction depending on the system.

VII. References

1. Pereira de Carvalho, Rodrigo, et al. Tuning the Electrochemical Properties of Organic Battery Cathode Materials: Insights from Evolutionary Algorithm DFT Calculations. vol. 13, 2020.
2. Grey, C., Tarascon, J. Sustainability and in situ monitoring in battery development. Nature Mater 16, 45–56 (2017). https://doi-org.ezproxy.its.uu.se/10.1038/nmat4777
3. Jouhara, Alia, et al. "Raising the Redox Potential in Carboxyphenolate-Based Positive Organic Materials Via Cation Substitution." *Nature Communications*, vol. 9, no. 1, 2018, pp. 4401-11.
4. Wang, S. et al. Organic Li4C8H2O6 nanosheets for lithium-ion batteries. Nano Lett. 13, 4404–4409 (2013).
5. Hohenberg P, Kohn W. 1964 Inhomogeneous electron gas. Phys. Rev. 136, B864–B871. (doi:10.1103/PhysRev.136.B864)
6. Armiento, Rickard, The Many-Electron Energy in Density Functional Theory (2005).
7. M. Born and J. R. Oppenheimer, Ann. Phys. 87, 457 (1927).
8. K. Capelle, A bird's-eye view of density-functional theory, http://arxiv.org/abs/cond-mat/0211443.
9. Kohn, W. (1995), Density functional theory for systems of very many atoms. Int. J. Quantum Chem., 56: 229-232. https://doiorg.ezproxy.its.uu.se/10.1002/qua.560560407
10. Hasnip PJ, Refson K, Probert MIJ, Yates JR, Clark SJ, Pickard CJ. Density functional theory in the solid state. *Philosophical transactions of the Royal Society of London. Series A: Mathematical, physical, and engineering sciences*. 2014;372:20130270-20130270.
11. Perdew JP, Burke K, Ernzerhof M. 1995 Generalized gradient approximation made simple. Phys. Rev. Lett. 77, 3865–3868. (doi:10.1103/PhysRevLett.77.3865)
12. Zhang, Qi & Khetan, Abhishek & Er, Süleyman. (2021). A quantitative evaluation of computational methods to accelerate the study of alloxazine-

derived electroactive compounds for energy storage. Scientific Reports. 11. 10.1038/s41598-021-83605-2.

13. K. N. Kudin and G. E. Scuseria, Phys. Rev. B 61, 16440 (2000)
14. Heyd J, Scuseria GE, Ernzerhof M. Hybrid functionals based on a screened Coulomb potential. *The Journal of chemical physics*. (2003)
15. Heyd J, Scuseria GE. Efficient hybrid density functional calculations in solids: assessment of the Heyd-Scuseria-Ernzerhof screened Coulomb hybrid functional. *The Journal of chemical physics*. (2004)
16. Adamo and V. Barone, J. Chem. Phys. 110, 6158 (1999)
17. J. P. Perdew, K. Burke, and M. Ernzerhof, Phys. Rev. Lett. 77, 3865 (1996)
18. L. A. Curtiss, K. Raghavachari, P. C. Redfern, and J. A. Pople, J. Chem. Phys. 106, 1063 (1997)
19. A. O. Lyakhov, A. R. Oganov, H. T. Stokes, Q. Zhu, Comput. Phys. Commun. 2013, 184, 1172 – 1182.
20. C. W. Glass, A. R. Oganov, N. Hansen, Comput. Phys. Commun. 2006, 175, 713 – 720.